



Star-forming galaxies at $z \approx 8\text{--}9$ from *Hubble Space Telescope*/WFC3: implications for reionization

Silvio Lorenzoni,¹★ Andrew J. Bunker,¹ Stephen M. Wilkins,¹ Elizabeth R. Stanway,² Matt J. Jarvis³ and Joseph Caruana¹

¹University of Oxford, Department of Physics, Denys Wilkinson Building, Keble Road OX1 3RH

²H. H. Wills Physics Laboratory, University of Bristol, Tyndall Avenue, Bristol BS8 1TL

³Centre for Astrophysics, Science & Technology Research Institute, University of Hertfordshire, Hatfield, Herts AL10 9AB

Accepted 2011 February 4. Received 2011 February 4; in original form 2010 June 18

ABSTRACT

We present a search for galaxies at $7.6 < z < 9.8$ using the latest *Hubble Space Telescope*/Wide Field Camera 3 (WFC3) near-infrared data, based on the Lyman-break technique. We search for galaxies which have large ($Y - J$) colours (the ‘ Y -drops’) on account of the Lyman α forest absorption, and with ($J - H$) colours inconsistent with being low-redshift contaminants. We identify 24 candidates at redshift $z \approx 8\text{--}9$ (15 are robust and a further nine more marginal but consistent with being high redshift) over an area of ≈ 50 arcmin 2 . Previous searches for Y -drops with WFC3 have focused only on the *Hubble Ultra Deep Field*, and our larger survey (involving two other nearby deep fields and a wider area survey) has trebled the number of robust Y -drop candidates. For the first time, we have sufficient $z \approx 8\text{--}9$ galaxies to fit both ϕ^* and M^* of the UV Schechter luminosity function. There is evidence for evolution in this luminosity function from $z = 6\text{--}7$ to $z = 8\text{--}9$, in the sense that there are fewer UV-bright galaxies at $z \approx 8\text{--}9$, consistent with an evolution mainly in M^* . The candidate $z \approx 8\text{--}9$ galaxies we detect have insufficient ionizing flux to reionize the Universe, and it is probable that galaxies below our detection limit provide a significant UV contribution. The faint-end slope, α , is not well constrained. However, adopting a similar faint-end slope to that determined at $z = 3\text{--}6$ ($\alpha = -1.7$) and a Salpeter initial mass function (IMF), then the ionizing photon budget still falls short if $f_{\text{esc}} < 0.5$, even integrating down to $M_{\text{UV}} = -8$. A steeper faint-end slope or a low-metallicity population (or a top-heavy IMF) might still provide sufficient photons for star-forming galaxies to reionize the Universe, but confirmation of this might have to await the *James Webb Space Telescope*.

Key words: galaxies: evolution – galaxies: formation – galaxies: high-redshift – galaxies: starburst – ultraviolet: galaxies.

1 INTRODUCTION

The $z \approx 8$ epoch is cosmologically very interesting: the Gunn-Peterson effect (Gunn & Peterson 1965; Scheuer 1965), the near total absorption of the continuum flux at wavelengths shorter than that of the Lyman α line due to a significant neutral hydrogen fraction in the intergalactic medium, has been observed at $z > 6.3$ in Sloan Digital Sky Survey quasi-stellar object spectra (Becker et al. 2001; Fan et al. 2001, 2006). This suggests that $z \approx 6$ lies at the end of the epoch of reionization, whose mid-point may have occurred at $z \approx 11$, according to latest results from *Wilkinson Microwave Anisotropy Probe* (Dunkley et al. 2009).

An outstanding problem, however, is what sources were responsible for the reionization of the Universe, and when exactly this occurred. There is evidence for old stellar populations in some $z \approx 4\text{--}6$ galaxies from Balmer break measurements in *Spitzer*/Infrared Array Camera (IRAC) imaging (Eyles et al. 2005, 2007; Stark et al. 2007, 2009), implying star formation commenced at even earlier times. Hence it is reasonable to consider the UV photons from this star formation as a possible cause of reionization. Age and stellar mass determinations of the above mentioned stellar populations are affected by many uncertainties, so is important to directly look for star formation at $z > 7$ to determine whether star-forming galaxies at these epochs can indeed provide the Lyman continuum photons required for reionization.

In recent years, observations of high redshift Universe ($z > 6$) have become possible. Deep imaging surveys with the *Hubble Space*

★E-mail: silvio.lorenzoni@astro.ox.ac.uk

Telescope (HST) and large ground-based telescopes have made the discovery of $z \approx 6$ galaxies almost routine. Some of those searches (Stanway, Bunker & McMahon 2003; Bunker et al. 2004; Yan & Windhorst 2004; Bouwens et al. 2006, 2007; Yoshida et al. 2006; Oesch et al. 2007) rely on the Lyman-break galaxy (LBG) technique, initially used by Steidel and collaborators (Steidel et al. 1996) to identify galaxies at $z \approx 3$ through the large absorption produced by the intervening Lyman α forest clouds and the Lyman limit. Until recently, working at higher redshift ($z > 7$) was challenging. Studies were limited to very small deep fields observed from space (e.g. Bouwens et al. 2008), or to extremely shallow wide-area surveys from the ground (e.g. Stanway et al. 2008; Hickey et al. 2010). The new Wide Field Camera 3 (WFC3) instrument, installed on *HST* in 2009 May, allowed this technique to be more effectively applied to $z \approx 7$ –10, thanks to its near-infrared channel with significantly larger field and better sensitivity than the previous-generation Near Infrared Camera and Multi-Object Spectrometer (NICMOS) instrument. Using WFC3 broad-band filters at 1.0, 1.25 and 1.6 μm (the Y , J and H bands) and targeting fields with existing deep Advanced Camera for Surveys (ACS) data, it is possible to identify optical ‘drop-outs’, objects seen only in the WFC3 infrared images but not in the optical ones. These are candidate $z \gtrsim 7$ galaxies. Searching for objects with no flux at 1.0 μm and below (Y -band drop-outs, or ‘ Y -drops’) could lead to the discovery of $z \approx 8$ galaxies. Deep optical images of the observed fields are still necessary to ‘clean up’ the list of candidates, because, as we will see later, optical detections are useful in ruling out many lower redshift contaminants.

The past few months have seen several papers presenting high-redshift galaxy candidates from *HST*/WFC3 imaging of the *Hubble Ultra Deep Field* (HUDF; Bunker et al. 2010; Finkelstein et al. 2010; McLure et al. 2010; Oesch et al. 2010; Bouwens et al. 2010a, Yan et al. 2010). In the HUDF, $\sim 10 z'$ -drops ($z \approx 7$) have been found, along with ~ 5 Y -drops ($z \approx 8$). Spectroscopic confirmation of these candidates in the HUDF will be extremely challenging, as they have magnitudes $J > 26.5$ (for the z' -drops) and $J > 28.0$ (for the Y -drops). What is needed are larger samples over wider areas, which might yield rarer but brighter candidates more suitable for spectroscopic follow-up. Such follow-up is important to test the validity of the Y -drop selection technique, and address the contaminant fraction, as well as exploring the physics of star-forming galaxies at $z \gtrsim 8$ (in particular whether Lyman α emerges during the Gunn–Peterson absorption era). Increasing the survey area of the WFC3 LBG searches will also improve the statistics [and hence the rest-UV luminosity function (rest-UVLF) constraints], and we have started to do this by searching for z' -drops in the larger area Early Release Science (ERS) WFC3 images of some of the Great Observatories Origins Deep Survey (GOODS)-South field (Wilkins et al. 2010) and expanding this to include two other deep flanking fields (UDF-P12 and UDF-P34) close to the HUDF (Wilkins et al. 2011a), which has increased the number of robust z' -drops from ~ 10 to ~ 40 . In this paper we use our new reductions of the ERS GOODS-South, and UDF-P12 and UDF-P34 to search for Y -drops at $z \approx 8$ –9. In Bunker et al. (2010), we presented our preliminary list of Y -drops in the HUDF, and here we also re-analyse this field using a more recent data reduction.

The evolution of the rest-UVLF is key to both understanding the star formation history of the Universe and also to address the role of star-forming galaxies in reionization. There seems to be strong evolution in the UVLF up to $z \approx 6$ (e.g. Stanway et al. 2003), and recent studies (Bunker et al. 2010; Wilkins et al. 2011a; Oesch et al. 2010) seem to show that this evolution continues up to $z \approx 7$, although based on small number statistics. Our goal is to

push the measurement of the UVLF further back in cosmic time by assembling a statistically significant sample of probable $z \approx 8$ –9 galaxies. From this we can address the evolution of the star formation rate (SFR) density, and the ionizing photon budget.

This paper is organized as follows. In Section 2 we outline the *HST* observations with WFC3 and the data reduction, and in Section 3 we describe our colour selection to recover high-redshift LBGs and compare our sample with those from other studies. In Section 4 we discuss the evolution of the SFR density and the implications for reionization, derived from the luminosity function we infer at $z \sim 8$. Our conclusions are presented in Section 5. Throughout, we adopt the standard concordance cosmology of $\Omega_M = 0.3$, $\Omega_\Lambda = 0.7$ and use $H_0 = 70 \text{ km s}^{-1} \text{ Mpc}^{-1}$. All magnitudes are on the AB system (Oke & Gunn 1983).

2 OBSERVATIONS AND DATA REDUCTION

2.1 Observations

In this paper we analyse images from WFC3 on *HST* taken in the near-infrared Y , J and H bands. The data come from two different *HST* programs, both covering areas within the GOODS-South field (Giavalisco et al. 2004). The *HST* Treasury programme GO-11563 (P.I. G. Illingworth) covers the HUDF and two nearby deep flanking fields (UDF-P12 and UDF-P34, also referred to as HUDF05-01 and HUDF05-02 in programme GO-11563). These flanking fields were imaged by the Advance Camera for Surveys (ACS) on *HST* in v , i' and z' bands during 2005–06 in parallel with deep *HST* NICMOS NIC3 observations of the original UDF as part of program GO-10632 (P.I. M. Stiavelli). In Bunker et al. (2010) we analysed the single-WFC3-pointing HUDF data obtained soon after the commissioning of WFC3, and in this paper we study the two new deep WFC3 pointings on the two deep flanking fields, and reanalyse the UDF data using more recent on-orbit calibration of the detector. Additionally, we analyse the ERS program GO/DD-11359 (P.I. R. O’Connell) data, covering 10 overlapping pointings with two orbits in each filter. An analysis of the first six pointings for z -drops at $z \approx 7$ was presented in Wilkins et al. (2010), with the full ERS mosaic and UDF-P12 and P34 flanking fields used to select z -drops in Wilkins et al. (2011a).

The infrared channel of WFC3 was used, which is a Teledyne 1014 \times 1014 pixel HgCdTe detector (a 10-pixel strip on the edge is not illuminated by sky and used for pedestal estimation), with a field of view of $123 \times 136 \text{ arcsec}^2$. Filters used in the two programs are the same for J and H bands ($F125W$ and $F160W$), while the ERS images use a Y -band filter ($F098M$) which covers only the blue side of the wider $F105W$ filter used in the UDF and flanking field images. The data were taken in ‘MULTIACCUM’ mode using SPARSAMPLE100, which non-destructively reads the array every 100 s. These repeated non-destructive reads of the infrared array allow gradient-fitting to obtain the count rate (‘sampling up the ramp’) and the flagging and rejection of cosmic ray strikes. For the HUDF and flanking fields (Programme GO-11563) there were two exposures per orbit, with each MULTIACCUM comprising 16 reads for a total duration of 1403 s per exposure. For the ERS images (Programme GO/DD-11359), there were three exposures per orbit, each with nine or 10 reads and with a total time of 803–903 s per exposure. In Table 1, we list the exposure time (and number of exposures) for each field and each spectral band. We note that for the Y -band images of the HUDF, two visits (eight exposures) were severely affected by image persistence, and as in Bunker et al. (2010) we exclude these from our data reduction.

Table 1. The total exposure time (in ks) is listed for each filter, with the number of individual exposures given in parentheses. The final columns give the 6σ and 7σ magnitude limits in the J band – the 6σ is the limit of our catalogue for candidate selection, and the luminosity function has been computed using Y -drops brighter than 7σ . All magnitudes are on the AB system, measured in a 0.6-arcsec diameter aperture with an aperture correction applied.

| WFC3 exposure times, in ks (number of exposures). | | | | | |
|---------------------------------------------------|---------------------|-----------|-----------|-------------|-------------|
| Field ID | Y band ^a | J band | H band | $J 6\sigma$ | $J 7\sigma$ |
| HUDF | 39.3 (28) | 44.9 (32) | 78.6 (56) | 28.51 | 28.34 |
| P34 | 28.1 (20) | 39.3 (28) | 47.7 (34) | 28.39 | 28.22 |
| P12 | 16.5 (12) | 33.2 (24) | 5.6 (4) | 28.31 | 28.14 |
| ERS | 5.0 (6) | 5.0 (6) | 5.0 (6) | 27.20 | 27.03 |

^a Y_{098m} for the ERS fields and Y_{105w} for the HUDF/P12/P34 fields.

2.2 Data reduction

The IRAF.STSDAS pipeline CALWFC3 was used to calculate the count rate and reject cosmic rays through gradient fitting, as well as subtracting the zeroth read and flat-fielding. We used MULTIDRIZZLE (Koekemoer et al. 2002) to combine exposures taken through the same filter in each pointing, taking account of the geometric distortions and mapping on to an output pixel size of 0.06 arcsec from an original 0.13 arcsec pixel⁻¹. This was the same scale as we used in our analysis of the HUDF WFC3 images (Bunker et al. 2010) and corresponds to a 2×2 block-averaging of the GOODSV2.0 ACS drizzled images.

The final frames had units of electrons per second, and we take the standard ACS zero-points for the UDF images. For WFC3, we use the recent zero-points reported on http://www.stsci.edu/hst/wfc3/phot_zp_lbn during 2010 February, where the $F098M$ Y band has an AB magnitude zero-point of 25.68 (such that a source of this brightness would have a count rate of 1 electron per second), and zero-points of 26.27, 26.25 and 25.96 for $F105W$, $F125W$ and $F160W$. We note that the information in the image headers of the earlier images released in 2009 September is slightly different by 0.1–0.15 mag, with zero-points of $F105W$ $Y_{zp} = 26.16$, $J_{zp} = 26.10$ and $H_{zp} = 25.81$ (as used in Bunker et al. 2010).

The new WFC3 images of fields UDF-P12 and UDF-P34 were reduced using the latest version of CALWFC3 (2009 October 29 release), and we also re-reduced the UDF images originally presented in Bunker et al. (2010) – the earlier paper had used a reduction using XDIMSUM and fits to the geometric distortion due to MULTIDRIZZLE not then being available for the newly commissioned WFC3. For the UDF and flanking fields, we used a pixel fraction of 0.6 to recover some of the undersampling. In each of these three fields, we survey 4.18 arcmin² in all exposures, with another 0.67 arcmin² surveyed at half the maximum depth in each field. For the ERS project, we reduced the data for all 10 pointings using the same technique as described in Wilkins et al. (2010; our analysis of the first six pointings). Here we used a pixel fraction of 1.0 in MULTIDRIZZLE, as we only had six exposures; a smaller pixel fraction would not fully populate the output repixelated grid with such a small number of exposures (this pixel fraction was also used for the H -band imaging of P12, as only four exposures had been taken at the time of writing – a small subset of the total still to be observed). We then mosaicked together the 10 ERS pointings in each filter, using inverse-variance weighting for the overlap regions, producing a field of fairly uniform depth covering 37 arcmin², with a further 8 arcmin² going less deep.

In our final combined J -band image, we measure a full width at half-maximum of ≈ 0.1 arcsec for point sources in the field. As most high-redshift galaxies are likely to be barely resolved (e.g. Bunker et al. 2004; Ferguson et al. 2004), we perform photometry using fixed apertures of 0.6-arcsec diameter, and introduce an aperture correction to account for the flux falling outside of the aperture. This correction was determined to be ≈ 0.2 –0.25 mag in WFC3 from photometry with larger apertures on bright but unsaturated point sources. We note that the H -band images display significant Airy diffraction rings around point sources. For the ACS images, the better resolution and finer pixel sampling require a smaller aperture correction of ≈ 0.1 mag. All the magnitudes reported in this paper have been corrected to approximate total magnitudes (valid for compact sources), and we have also corrected for the small amount of foreground Galactic extinction towards these fields using the COBE/DIRBE and IRAS/ISSA dust maps of Schlegel, Finkbeiner & Davis (1998). The optical reddening is $E(B-V) = 0.009$, equivalent to extinctions of $A_{850p} = 0.012$, $A_{105w} = 0.010$, $A_{125w} = 0.008$ and $A_{160w} = 0.005$.

The geometric transformation and image re-gridding produces an output where the noise is highly correlated, hence measuring the standard deviation in blank areas of the final drizzled image will underestimate the noise. To ascertain the true significance of object detections, we determine the real noise using several different techniques. As in Bunker et al. (2010), we also produced a crude combination of the individual flat-fielded images using integer-pixel shifts. While this was not used for our science (as the significant geometric distortions were not accounted for, and it did not address the undersampling of the point spread function as ‘drizzle’ does), this output frame had the advantage that the noise properties were preserved and adjacent pixels were uncorrelated. We measured the standard deviation of the counts in blank areas of sky in this shift-and-add mosaic, and we verified that the noise (normalized per unit time) decreased as the square root of the number of frames combined. The limiting magnitudes found using these uncorrelated ‘true-noise frames’ are in good agreement with the STScI HST/WFC3 Exposure Time Calculator (ETC) – Table 2 presents our 2σ limits in a 0.6-arcsec diameter aperture, with the aperture correction applied. We also produced a noise model based on the detector gain, readout noise and Poisson counts of the measured background (including the instrument dark current), and verified that our sensitivity was well within 10 per cent of the expected noise. Finally, we measure the correlated noise (the standard deviation of the background counts) in the drizzled image mosaics which we use for our source detection and photometry, and use the relations in equation (A13) of Casertano et al. (2000) to introduce a correction factor which depends on the output pixel scale and the size of the ‘droplet’ in the drizzling procedure (‘pixfrac’). We generally found good agreement (at the 0.05 mag level) with our sensitivity measurements using the true-noise frames, except for the HUDF data where the corrected drizzle noise underestimated the true noise by 0.1–0.2 mag, perhaps because of the large number of frames combined with small subpixel shifts. We adopted the sensitivity measurements from the true-noise frame, having checked that consistent results were produced by the ETC, the noise model and the noise in the drizzle frame corrected for pixel correlations. Our measured noise in the HUDF is in good agreement with Bouwens et al. (2010a), but we note that McLure et al. (2010) appear to be ≈ 0.3 mag less sensitive (although we note that their 5σ magnitude limit in a 0.4-arcsec diameter aperture appears not to have been corrected to total magnitudes with an aperture correction, unlike in Bouwens et al. 2010a).

Table 2. Summary of observations. All magnitudes are on the AB system, and measured in a 0.6-arcsec diameter aperture with an aperture correction applied to correct to approximate total flux (for compact sources).

| Field ID | Centre (J2000) | ACS/WFC3 2 σ detection limits (AB magnitudes) | | | | | | | |
|----------|----------------------|------------------------------------------------------|------------|------------|------------|------------|-------------------|------------|------------|
| | | Area (arcmin 2) | b_{435w} | v_{606w} | i_{775w} | z_{850p} | $Y_{098m/105w}^a$ | J_{125w} | H_{160w} |
| HUDF | 03:32:38.4 –27:47:00 | 4.2 | 30.3 | 30.7 | 30.6 | 30.0 | 29.65 | 29.70 | 29.67 |
| P34 | 3:33:05.3 –27:51:23 | 4.2 | – | 29.9 | 29.5 | 29.7 | 29.45 | 29.58 | 29.41 |
| P12 | 3:33:01.9 –27:41:10 | 4.2 | – | 29.9 | 29.6 | 29.6 | 29.16 | 29.50 | 28.23 |
| ERS | 3:32:23.6 –27:42:50 | 37.0 | 29.1 | 29.1 | 28.5 | 28.4 | 28.02 | 28.39 | 28.10 |

^a Y_{098m} for the ERS field and Y_{105w} for the HUDF/P12/P34 fields.

The optical *HST*/ACS imaging comes from the HUDF (Beckwith et al. 2006), and we used the publicly available v , i , z reductions of flanking field UDF-P12 provided by the UDF05 team (Oesch et al. 2007). We reduced the v , i , z ACS data for UDF-P34 from the *HST* archive, using MULTIDRIZZLE to combine a large subset of the data comprising blocks of data taken close in time with similar telescope roll angles, again using an output 0.03 arcsec pixel $^{-1}$ scale. These subsets of drizzled images were then registered and combined with IRAF.IMCOMBINE. Our combined images were 4.8 ks in v band, 10.6 ks in i band and 26.8 ks in z band. All the ACS images were then block-averaged 2×2 and registered with our drizzled WFC3 frames.

2.3 Construction of catalogues

To perform the candidate selection we used the SExtractor photometry package (Bertin & Arnouts 1996), version 2.5.0. Since we are searching for Y -drops (objects clearly detected in the WFC3

J band but with minimal flux in the Y band and ACS images), fixed circular apertures 0.6 arcsec in diameter were ‘trained’ in the J image, and running SExtractor in dual-image mode those apertures were used to measure the flux in the same locations in the Y -band image. The same procedure was repeated between J -band image and all the other ACS and WFC3 images with different filters. For each waveband we used a weight image derived from the exposure map. To identify the objects, we set the SExtractor parameters to have a lower limit of five contiguous pixels above a threshold of 2σ per pixel (data were drizzled to a scale of 0.06 arcsec pixel $^{-1}$). We corrected the aperture magnitudes to approximate total magnitudes with the aperture correction appropriate for that filter. With this cut we were able to detect all significant sources, along with some spurious detections just above the noise limit or due to diffraction spikes from stars. We also impose a 6σ limit on the J -band magnitude for all fields, with the J_{AB} magnitude limit listed in the last column of Table 1. Table 3 presents our photometry of Y -drops

Table 3. Y -band drop out candidate $z \approx 8$ –9 galaxies meeting our selection criteria in the HUDF, P12, P34 and ERS fields. Objects are divided by field and then ordered by apparent J_{AB} magnitude. Where the measured flux is $<1\sigma$, an upper limit at the 1σ level is quoted. The significance of the J -band detection is shown in parentheses after the magnitude. Objects marked with ‘*’ are more marginal candidates; see Section 3.2. The ERS field uses the narrower Y -band filter $F098M$, and the other fields use $F105W$. For the P34 field, we introduce a small offset to the astrometry in the *HST* image headers (given in Lorenzoni et al. <http://arxiv.org/abs/1006.3545v1>) of $\Delta RA = 0.03$ to match the astrometry from GSC-2 and Two Micron All Sky Survey.

| ID | RA | Dec. | Y_{AB} | J_{AB} (significance, σ) | H_{AB} | $(Y - J)_{AB}$ | $(J - H)_{AB}$ |
|----------|--------------|--------------|------------------|------------------------------------|------------------|----------------|----------------|
| HUDF.YD2 | 03:32:37.796 | –27:46:00.12 | >29.76 | 28.08 ± 0.12 (8.9 σ) | 28.20 ± 0.14 | >1.66 | –0.12 |
| HUDF.YD1 | 03:32:42.873 | –27:46:34.58 | 29.25 ± 0.37 | 28.15 ± 0.13 (8.3 σ) | 28.15 ± 0.13 | 1.10 | 0.00 |
| HUDF.YD3 | 03:32:38.135 | –27:45:54.03 | 29.79 ± 0.61 | 28.18 ± 0.13 (8.1 σ) | 28.10 ± 0.13 | 1.61 | 0.08 |
| HUDF.YD4 | 03:32:33.130 | –27:46:54.49 | 29.85 ± 0.65 | 28.32 ± 0.15 (7.1 σ) | 29.29 ± 0.38 | 1.53 | –0.97 |
| HUDF.YD8 | 03:32:43.082 | –27:46:27.75 | 29.75 ± 0.59 | 28.45 ± 0.17 (6.3 σ) | 28.84 ± 0.25 | 1.30 | –0.39 |
| HUDF.YD9 | 03:32:36.360 | –27:46:23.35 | 29.78 ± 0.61 | 28.50 ± 0.18 (6.1 σ) | 28.43 ± 0.17 | 1.28 | 0.07 |
| P34.YD1 | 03:33:00.340 | –27:51:20.97 | 29.71 ± 0.68 | 27.94 ± 0.12 (9.1 σ) | 28.27 ± 0.19 | 1.77 | –0.33 |
| P34.YD2 | 03:33:09.657 | –27:51:16.45 | 29.89 ± 0.81 | 27.95 ± 0.12 (9.0 σ) | 27.61 ± 0.10 | 1.94 | 0.34 |
| P34.YD3 | 03:33:07.474 | –27:51:14.89 | 29.85 ± 0.78 | 28.07 ± 0.14 (8.1 σ) | 28.86 ± 0.33 | 1.78 | –0.79 |
| P34.YD4 | 03:33:04.857 | –27:51:38.28 | 29.36 ± 0.50 | 27.89 ± 0.11 (9.5 σ) | 27.83 ± 0.13 | 1.47 | 0.06 |
| P34.YD5* | 03:33:06.596 | –27:52:48.95 | >30.20 | 28.29 ± 0.17 (6.6 σ) | 28.20 ± 0.18 | >1.91 | 0.09 |
| P34.YD6 | 03:33:06.901 | –27:51:32.54 | 29.69 ± 0.67 | 28.35 ± 0.18 (6.2 σ) | 28.03 ± 0.15 | 1.34 | 0.32 |
| P34.YD7* | 03:33:09.286 | –27:51:32.22 | >29.91 | 28.38 ± 0.18 (6.1 σ) | 28.85 ± 0.32 | >1.53 | –0.47 |
| P12.YD1* | 03:33:03.034 | –27:41:57.00 | 29.64 ± 0.84 | 28.01 ± 0.14 (7.9 σ) | >28.98 | 1.63 | <–0.97 |
| P12.YD2* | 03:33:00.545 | –27:41:46.80 | 29.25 ± 0.59 | 28.03 ± 0.14 (7.8 σ) | >28.44 | 1.22 | <–0.41 |
| ERS.YD1 | 03:32:23.369 | –27:43:26.53 | >28.77 | 26.98 ± 0.15 (7.3 σ) | 27.87 ± 0.43 | >1.79 | –0.89 |
| ERS.YD2* | 03:32:02.986 | –27:43:51.95 | >28.39 | 26.98 ± 0.15 (7.3 σ) | 26.86 ± 0.17 | >1.41 | 0.12 |
| ERS.YD3 | 03:32:29.790 | –27:43:01.09 | >28.77 | 27.03 ± 0.16 (7.0 σ) | 27.83 ± 0.42 | >1.74 | –0.80 |
| ERS.YD4 | 03:32:40.904 | –27:40:12.37 | >28.77 | 27.06 ± 0.16 (6.8 σ) | 27.96 ± 0.47 | >1.71 | –0.90 |
| ERS.YD5* | 03:32:18.414 | –27:43:45.99 | >28.77 | 27.06 ± 0.16 (6.8 σ) | 27.35 ± 0.27 | >1.71 | –0.29 |
| ERS.YD6 | 03:32:05.022 | –27:45:53.93 | 28.61 ± 0.91 | 27.19 ± 0.18 (6.1 σ) | 27.38 ± 0.28 | 1.42 | –0.19 |
| ERS.YD7* | 03:32:41.676 | –27:41:27.48 | >28.03 | 26.95 ± 0.14 (7.6 σ) | 26.56 ± 0.13 | >1.08 | 0.39 |
| ERS.YD8* | 03:32:37.927 | –27:42:20.78 | >28.14 | 27.14 ± 0.17 (6.3 σ) | 26.89 ± 0.18 | >1.00 | 0.25 |
| ERS.YD9* | 03:32:27.014 | –27:44:31.29 | >28.57 | 27.20 ± 0.18 (6.0 σ) | 27.85 ± 0.43 | >1.37 | –0.65 |

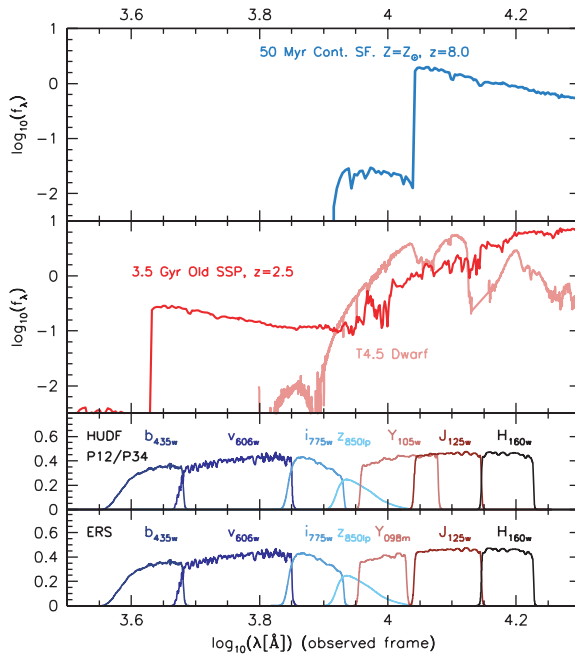


Figure 1. Top panel: model (from the Starburst99; Leitherer et al. 1999) SED of a redshifted $z = 8$ star-forming galaxy. Middle panel: potential contaminants – observed SED of a low-mass dwarf star (class: T4.5; Knapp et al. 2004) together with the model (Starburst99) SED of a 3.5-Gyr SSP at $z = 2.5$. The bottom two panels show the transmission functions of the combination of filters available to each field.

from SExtractor, where we have corrected the magnitude errors returned by SExtractor for the effects of correlated noise in the drizzled images, using our ‘true-noise frames’ to determine the scaling factor (typically SExtractor underestimated the magnitude errors by a factor of ≈ 1.5 for $\text{pixfrac} = 0.6$ used in most of our data, and a factor of ≈ 2.6 for $\text{pixfrac} = 1.0$ as used in the ERS and the H band of P12).

3 CANDIDATE SELECTION

Identification of candidates is achieved using the Lyman-break technique (e.g. Steidel et al. 1996), where a large colour decrement is observed between filters either side of Lyman α in the rest-frame of the galaxy. At $z > 6$, the flux decrement comes principally from the large integrated optical depth of the intervening absorbers (the Lyman α forest).

At $z \approx 8-9$, the location of the Lyman α break is redshifted to $\sim 1.1\mu\text{m}$ – the WFC3 $Y_{105w/098m}$ and J_{125w} are suitably located such that a $7.6 < z < 9.8$ star-forming galaxy will experience a significant flux decrement between these two filters (see Figs 1 and 5), although the selection efficiency drops at the extremes of this range.

3.1 Contamination

Searching for distant galaxies using only broad-band photometry means that contamination is a potentially serious issue. There are two main sources of contamination: objects whose intrinsic colours are similar to those of the target population and faint objects with intrinsically different colours but whose observed colours scatter into our selection because of photometric noise. We note that the effect of transient phenomena is not significant for the selection of

Y -drops, since the WFC3 Y , J and H images were taken close in time. This is unlike our selection of z' -drops (e.g. Bunker et al. 2010; Wilkins et al. 2010; Wilkins et al. 2011a) where the ACS z' -band and WFC3 Y -band were separated by many years, so a transient such as a supernova or high-proper-motion object which entered the Y band but was absent at that location in the ACS could be erroneously identified as a LBG. Indeed, a probable supernova was identified in the WFC3 imaging of the HUDF (e.g. Bunker et al. 2010).

3.1.1 Intrinsically red objects

There are two distinct types of objects whose apparent $Y_{105w/098m} - J_{125w}$ colours are similar to those of LBGs at $z \approx 8$: lower redshift ($z \approx 2$) galaxies have the Balmer/4000-Å break feature between the two filters used, $Y_{105w/098m}$ and J_{125w} , while some low-mass dwarf stars, especially those of L and T spectral class, have low temperatures and broad absorption features that can mimic a spectral break.

Examples of the spectral energy distributions (SEDs) of each of these types of object [a model 3.5-Gyr old single-aged stellar population (SSP) at $z = 2.5$ and a T4.5 dwarf star] are shown in Fig. 1. In the case of lower redshift galaxies, the slope of the SED longwards of the spectral break (i.e. longwards of $Y_{105w/098m}$) is somewhat redder than that predicted for a high- z star-forming galaxy. The addition of a further filter at wavelengths redder than the J_{125w} filter (H_{160w} in this case) can then be used to discriminate between high- z and lower redshift galaxies (Fig. 2). L and T dwarfs contamination in the HUDF and P34 field is mostly ruled out by the $Y_{105w} - J_{125w}$ colour selection we adopted. The addition of H_{160w} photometry is still important in excluding these objects in the ERS field (see Fig. 3), where the different Y -band filter used provides less good discrimination using $Y - J$ colour alone.

In Figs 2 and 3 the positions of both the interlopers and the tracks expected for high-redshift star-forming galaxies are shown in the $(J_{125w} - H_{160w}) - (Y_{105w/098m} - J_{125w})$ colour plane. With the exception of the lowest temperature T dwarfs where the Y_{098m} filter is employed (the ERS field), these interlopers form a distinct locus separate from $z \approx 8-9$ star-forming galaxies with UV spectral slope index $\beta < 0.0$ (where $f_\lambda = \lambda^\beta$ is used as a model of the UV properties of star-forming galaxies).

Using this analysis, it is possible to design a window in $(Y_{105w/098m} - J_{125w}) - (J_{125w} - H_{160w})$ colour–colour space that selects mainly high-redshift star-forming galaxies, while eliminating known contaminant populations. For the HUDF/P12/P34 fields (i.e. where we have Y_{105w} imaging), this YJH selection criteria is

$$(Y_{105w} - J_{125w}) > 0.9$$

$$(Y_{105w} - J_{125w}) > 0.73(J_{125w} - H_{160w}) + 0.9$$

$$(J_{125w} - H_{160w}) < 1.5.$$

The use of an alternative Y filter (Y_{098m}) in the ERS field necessitates the use of a slightly different criteria:

$$(Y_{098m} - J_{125w}) > 0.9$$

$$(Y_{098m} - J_{125w}) > 0.64(J_{125w} - H_{160w}) + 1.28$$

$$(J_{125w} - H_{160w}) < 0.8.$$

We have designed our selection criteria to reject all known interlopers, while selecting most $z \approx 8-9$ star-forming galaxies. Other groups have used similar colour:colour selection, but with slightly

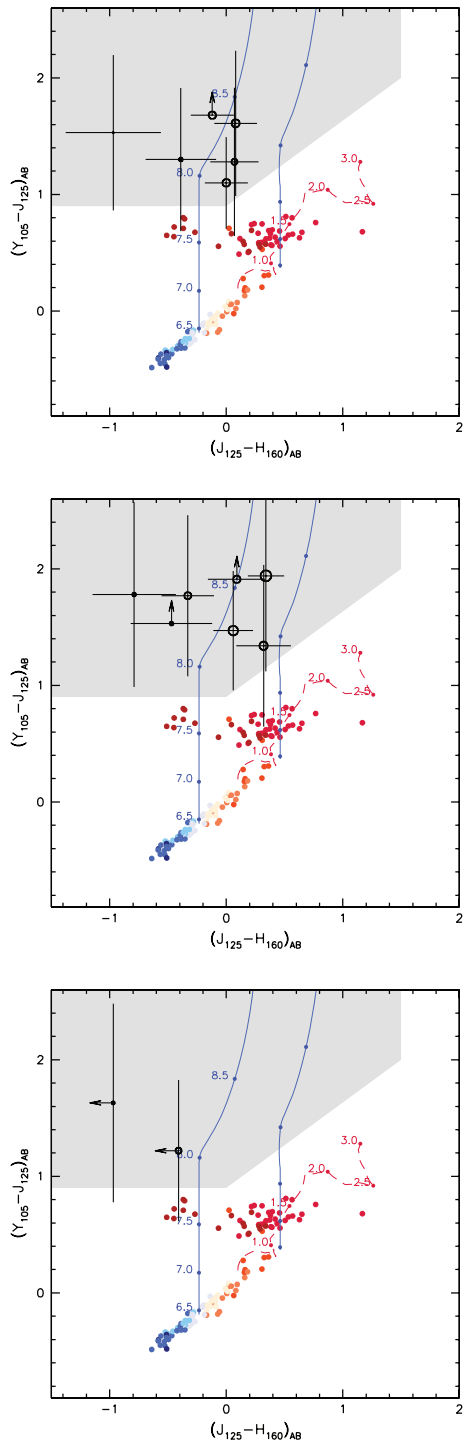


Figure 2. $J_{125w} - H_{160w}$ and $Y_{105w} - J_{125w}$ colour–colour figures for the HUDF (top) and flanking fields P34 (middle) and P12 (bottom), showing our YJH colour selection window (grey shaded area), the location of our candidates, the predicted paths taken by high-redshift galaxies (solid lines, $\beta = -3.0$, left and $\beta = 0.0$, right) and the location of possible contaminating sources. Contaminating sources include Galactic stars ($O - T$ dwarf stars, with L and T stars being redder, denoted by filled circles) and a passively evolving ‘early-type’ galaxy (modelled as an instantaneous burst of star formation at $z = 10$ followed by passive luminosity evolution, denoted by the dashed line). High-redshift candidates are denoted by black open circles (where the size of the circle is an indication of the apparent J_{AB} magnitude, with bigger circles indicating brighter sources). Limits and error bars are 1σ .

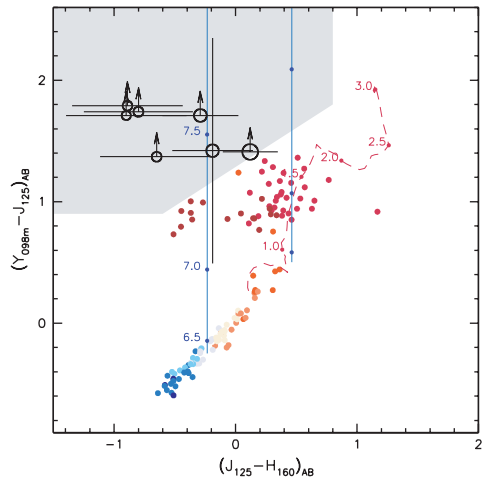


Figure 3. $J_{125w} - H_{160w}$ and $Y_{098m} - J_{125w}$ colour–colour figures for the ERS field showing our YJH colour selection window (grey shaded area), the location of our candidates, the predicted paths taken by high-redshift galaxies (solid lines, $\beta = -3.0$, left and $\beta = 0.0$, right) and the location of possible contaminating sources. Contaminating sources include Galactic stars (denoted by filled circles) and a passively evolving instantaneous burst of star formation that occurred at $z = 10$ (dashed line). High- z candidates are denoted by black open circles (where the size of the circle is an indication of the apparent J_{AB} magnitude, with the brighter sources being bigger circles). Limits and error bars are 1σ . Objects ERS.YD7 and ERS.YD8 are very marginal and hence not included in this figure (see Section 3.2).

different colour cuts (e.g. Bouwens et al. 2010a). Although this may affect the surface density of candidates (due to a slightly different redshift range and spectral range of spectral slopes probed for the LBGs, and a different contaminant fraction), the inferred luminosity functions should be similar as these selection effects are corrected for in the effective volume calculation. The window we obtain with such criteria excludes a hypothetical population of $z \approx 8-9$ galaxies with $J_{125w} - H_{160w} \gtrsim 1$ colours. Such a population would have extremely red UV spectral slopes, possibly due to massive dust reddening. The potential bias of our selection criteria and a more general analysis of the UV properties of the candidates presented in this work are discussed in more detail in Wilkins et al. (2011b), where we conclude that the distribution of UV spectral slope indices is consistent with being blue, with $\beta \approx -2$.

3.1.2 Photometric scatter

Even with the selection criteria described above, we cannot prevent some objects being scattered into our selection window because of photometric noise. At low signal-to-noise ratio, this contamination could be significant, and we impose another criterion to exclude those objects. To do that we use the deep optical imaging available in the ACS b_{435w} , v_{606w} , i_{775w} and z_{850lp} bands: because of the strong Lyman α forest absorption, $z \approx 8-9$ galaxies should not have any significant flux in the b_{435w} , v_{606w} and i_{775w} bands, so we impose an additional *byi non-detection* criteria for the selection of our candidates. All objects with a $>2\sigma$ detection in any of the b_{435w} , v_{606w} and i_{775lp} are classified as contaminants. The depths of these ACS images are given in Table 2. We note that the z_{850w} filter does have a red tail which overlaps with the $Y_{098m/105w}$ -band filters used, so it is conceivable that a Y -drop towards the lower end of the redshift selection might have residual z -band flux. However, we found only one Y -drop (P34.YD5) with a $\sim 2\sigma$ detection in z band.

3.2 Candidate galaxies at $z \approx 8$ –9

After imposing our selection criteria we are able to compile a list of candidate $z \approx 8$ –9 star-forming galaxies in the HUDF, UDF-P34, UDF-P12 and ERS fields. In Table 3 we list positions and photometry of these objects, while thumbnails of the $bvizYJH$ images of these candidates (where available) are presented in Fig. 4. In total we find 24 Y -drop candidates (HUDF:6, UDF-P34:7, UDF-P12:2, ERS:9) covering a range of apparent J_{AB} magnitudes of 27.0–28.5. In the three deep single WFC3 pointings, the number of candidates is fairly consistent from field to field, with 3, 4 and 2 Y -drops for the HUDF, UDF-P34 and UDF-P12 fields, respectively, at $J_{AB} < 28.2$.

There are nine (of the 24) objects in the Y -drop list (Table 3) which we flag as being more marginal than the other candidates as they sit at the limits of our selection, although they are plausible $z \approx 8$ –9 galaxies (our effective volume calculation already corrects for galaxies excluded as lying just outside the selection region). Candidates ERS-YD7 and ERS-YD8 in the ERS are flagged, as we only have a lower limit on the $(Y - J)$ colour (they are $\lesssim 1\sigma$ in Y band). Adopting the 1σ lower limit on the $(Y - J)$ colour places them in or above the ‘contaminant’ triangular region of Fig. 2, fully consistent with entering our selection area. Similarly, objects ERS-YD2, ERS-YD5, ERS-YD9 and P34-YD7 are flagged: using a 1σ lower limit on the $(Y - J)$ colour these candidates would fully meet our selection criteria (see Figs 2 and 3), while a more conservative 2σ lower limit could potentially locate them just below our selection box, although with colours consistent with falling within the selection window. Deeper Y -band imaging is required to show unambiguously that they are not in the ‘contaminant’ region of the colour:colour space. Object P34-YD5 in P34 is also flagged, because it has a $\sim 2\sigma$ detection in the z band. There are no detections in v -, i - and Y bands, though, so it is still a likely high-redshift ($z > 6$) object – the z -band flux might be statistical fluctuation or perhaps a high-equivalent-width emission line within the z band.

We also flag as marginal two potential high-redshift galaxies in field UDF-P12, on the grounds that the short exposure time of the H -band image in this field (Table 1) made it impossible to measure the H_{AB} magnitude. The upper limits on the $(J - H)$ colours place them away from the red contaminant region with $(J - H) > 1.5$ (Fig. 2), but we require the UV luminosity in the H filter (uncontaminated by the effects of Lyman α forest absorption) to infer the absolute UV magnitude (as described in Section 4.1). We now consider whether these single-band detections might be due to transients (such as was the case for the likely supernova in the WFC3 images of the HUDF, object zD0 in Bunker et al. 2010). The P12 field was observed in J band in two observing blocks, with eight frames taken on UT 2009 November 02, and the other 16 frames taken over UT 2009 November 10–15. As a check, we combined the two different epochs separately with ‘MULTIDRIZZLE’. The magnitude of P12-YD1 is consistent between the two epochs, with $J = 28.07 \pm 0.25$ (4.3σ) and $J = 27.95 \pm 0.16$ (6.8σ), respectively. However, P12-YD2 might show some variability in the J band with $J = 27.36 \pm 0.13$ (8.3σ) for the first block of data and $J = 28.14 \pm 0.19$ (5.8σ) for the second. Hence it is plausible that P12-YD2 might be a transient rather than a high-redshift Y -drop. When this WFC3 program (GO-11563) is complete, the H band will be much deeper on P12, allowing a further check on the robustness of the candidates in this field. However, the two candidates in P12 represent less than 10 per cent of our Y -drop sample, so will not quantitatively affect our conclusions; for the moment, we exclude this field from our fitting of the UVLF.

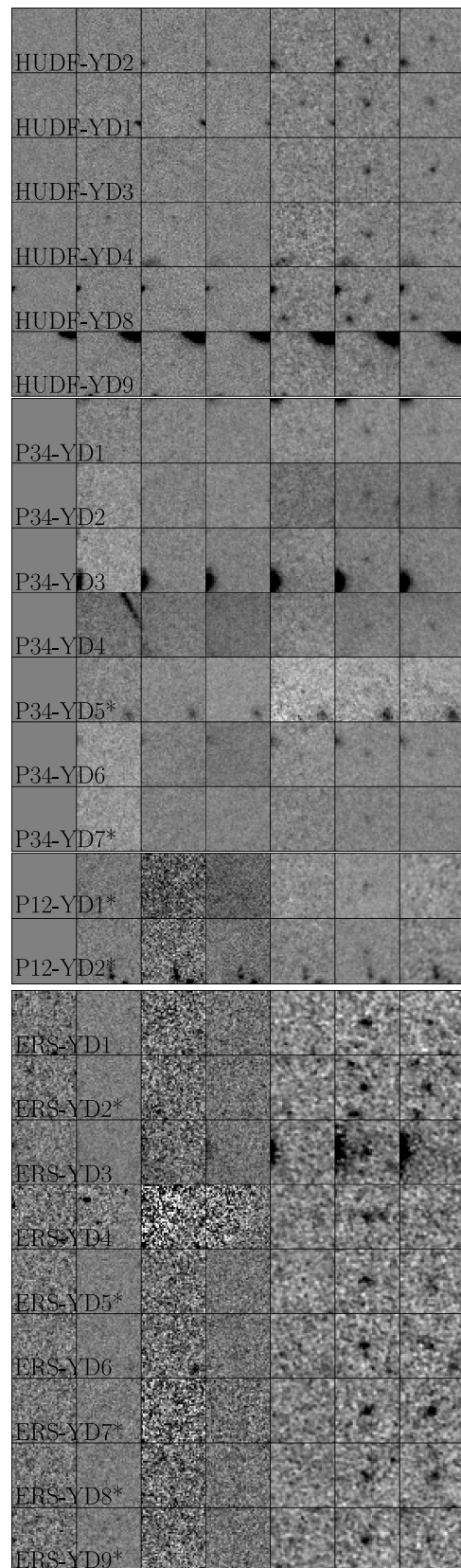


Figure 4. $2.4 \times 2.4 \text{ arcsec}^2$ $(b)vizYJH$ thumbnail images of objects meeting our selection criteria in the analysed fields. Within each field they are ordered by H -band magnitude (brightest at the top). Objects marked with $*$ are more marginal candidates; see Section 3.2. The fields UDF-P12 and UDF-P34 do not have ACS b -band imaging.

3.3 Comparison with other studies

We now compare our new list of candidates within the HUDF field with other groups' previous studies (Oesch et al. 2010; Bouwens et al. 2010a; Finkelstein et al. 2010; McLure et al. 2010; Yan et al. 2010), and particularly with our previous paper (Bunker et al. 2010). A matched catalogue between the Bunker et al. (2010), McLure et al. (2010) and Bouwens et al. (2010a) samples has already been presented in Bunker & Wilkins (2009).

Our refined HUDF sample, based on a new reduction of the HUDF data, has six Y -band drop-outs. In Bunker et al. (2010), we presented a list of seven Y -drop candidates within the HUDF field, the brightest four (in J band) of which are reproduced with the new selection (HUDF-YD1,2,3 and 4). Of the three other Y -drops from Bunker et al. (2010), one (YD5) has a discrepant $(Y_{105w} - J_{125w}) = 0.2$ colour in the new data reduction, much bluer than our selection criteria of $(Y_{105w} - J_{125w}) > 0.9$. The faintest Y -drop in Bunker et al. (2010), YD7, is marginally too faint ($J = 28.65$) in our new reduction of the HUDF images to enter our new sample. However, applying our new colour selection criteria to the old photometry (where $J = 28.44$) would have resulted in the selection of YD7. The remaining one (YD6) is only marginally too blue for the Lyman-break selection in the newly reduced data, with $(Y_{f105w} - J_{f125w}) = 0.89$, very close to the $(Y_{f105w} - J_{f125w}) > 0.9$ cut. This object has slight ($\sim 2\sigma$) detections in the ACS bands, too, and does not meet the selection criterion $(Y_{105w} - J_{125w}) > 0.73(J_{125w} - H_{160w}) + 0.9$, so we did not include it in our list. Moreover, no other group has found or listed this object as a candidate.

Two objects in our new catalogue (HUDF.YD8 and HUDF.YD9) were not found in Bunker et al. (2010); our previous study of Y -drops in the HUDF used slightly different magnitude and colour cuts [$J_{AB} < 28.5$ and $(Y - J)_{AB} > 1.0$], and an older reduction and photometric zero-points. These two objects were slightly too faint in the previous version of our HUDF reductions ($J = 28.59$ and 28.55, respectively) and slightly too blue ($(Y_{f105w} - J_{f125w}) = 0.77$, 0.92 respectively) to be selected with our original criteria in Bunker et al. (2010). The new candidate HUDF.YD8 lies only 1 arcsec from the z -drop zD5 in Bunker et al. (2010), and it is conceivable that both objects might be physically associated and might have similar redshifts at $z \sim 8$. We note that no other group has identified HUDF.YD9 as a candidate.

In Table 4 we show the Y -drop galaxy candidates from our HUDF catalogue which have been previously reported with their corresponding catalogue names from other groups, while in Table 5 we show all the objects found by these groups with colours or photometric redshifts compatible with being in our Y -drop redshift range, but which do not appear in our new catalogue. We mark with a ‘†’ the candidates that would be within our selection window if we adopt the photometry originally presented in the discovery papers,

Table 4. A list of Y -drops in the HUDF appearing in the catalogues of all previous analyses. We show in columns the different candidate ID used in this paper, in Bo10 (Bouwens et al. 2010a), Bu10 (Bunker et al. 2010), M10 (McLure et al. 2010), Y10 (Yan et al. 2010) and F10 (Finkelstein et al. 2010).

| ID | Bo10 | Bu10 | M10 | Y10 | F10 |
|----------|---------------|------|-------|---------|-----|
| HUDF-YD2 | UDFy-37796000 | YD2 | 1939y | z8-B117 | 200 |
| HUDF-YD1 | UDFy-42886345 | YD1 | 1765y | z8-B092 | 819 |
| HUDF-YD3 | UDFy-38135539 | YD3 | 1721y | z8-B115 | 125 |
| HUDF-YD4 | – | YD4 | 2487 | – | – |
| HUDF-YD8 | UDFy-43086276 | – | 2841y | z8-B088 | 653 |

rather than remeasuring this with our new reduction of the HUDF WFC3 imaging and the latest photometric zero-points.

Most of the other HUDF candidates from different groups do not meet our selection criteria both because they are too faint in the J band (class A in the Table 5) and because they are too blue, $(Y_{105w} - J_{125w}) < 0.9$ (class B in the Table 5). Only one candidate (z8-SB27 in Yan et al. 2010) meets our selection criteria for brightness in the J band and the $(Y_{105w} - J_{125w})$ colour, but is rejected on the basis of its location in the $J - H:Y - J$ colour:colour plane as a likely lower redshift Balmer-break galaxy (see Fig. 2). This galaxy is classified with letter ‘C’ in the table. We note that Bouwens' candidate UDFy-37636015 (our YD7) has inconsistent photometry presented in Bouwens et al. (2009) and Bouwens et al. (2010a) – adopting the more recent photometric values from Bouwens et al. (2010a), YD7 would enter our Y -drop selection (Table 5).

In summary, using our latest reduction of the WFC3 images of the HUDF we are able to reproduce four of the seven Y -band drop-out galaxies we first reported in Bunker et al. (2010); of two additional Y -drops in the new analysis, one has been reported elsewhere and one is a new discovery in the HUDF field. Remeasuring the photometry of Y -drop candidates presented elsewhere by other groups, we find that most would not enter our selection as they are too faint in J band and/or are too blue in $(Y - J)$, and hence are not as robust candidate $z \approx 8$ –9 galaxies as our core sample.

Table 5. List of candidates from other studies of the HUDF (see Table 4) quoted by respective authors to be either a Y -drop or in our redshift range ($7.6 < z < 9.8$, see Section 3) but that we do not recover. Class A denotes objects too faint in J band ($J_{AB} > 28.51$). Class B means that the colour selection criterion $(Y_{105w} - J_{125w}) > 0.9$ was not met. Class C is where the $(J - H):(Y - J)$ colour:colour rules out selection [i.e., $(Y_{105w} - J_{125w}) > 0.73(J_{125w} - H_{160w}) + 0.9$ is not met]. Objects marked ‘†’ would meet our selection criteria if we adopt the original photometry (but which do not make our selection if we use the photometry from our new reduction of the imaging data).

| Bunker'10 | M10 | F10 | Y10 | Bo10 | Class |
|-----------|------------------|----------|--------------|-----------|---------|
| YD5† | – | – | z8-SD24 | – | AB |
| YD6† | – | – | – | – | – |
| YD7† | 2079y 1107z** | 213 – | z8-B114 – | y37636015 | AB B |
| – | 1422 | 2055 | z8-B041c† | – | B |
| – | – | 800* | – | – | B |
| – | – | 3022 | – | – | AB |
| – | – | 640 | – | – | B |
| – | – | – | z8-B094† | – | – |
| – | – | – | z8-B087† | – | – |
| – | – | – | z8-SB27 | – | C |
| – | – | – | z8-SB30 | – | B |
| – | – | – | z8-SD05 | – | AB |
| – | – | – | z8-SD02 | – | AB |
| – | – | – | z8-SD15 | – | AB |
| – | – | – | z8-SD52 | – | AB |

† Object that would meet our selection criteria, assuming original photometry.

* Object 800 appears in versions 1, 2 and 3 of the arXiv:0912.1338 version of Finkelstein et al. (2010), but is absent from version 4 and the Astrophysical Journal paper.

** Object also found by Oesch et al. (2009 b), named UDFz-44716442, and classified as a z -drop. We included this object in our table since McLure et al. (2010) quote a photometric redshift of 7.60, on the edge of our selection range.

4 DISCUSSION

4.1 The luminosity function of Y -drops at $z \approx 8-9$

From the observed surface density of Y -drops, as a function of magnitude, we can recover the luminosity function of $z \approx 8-9$ galaxies in the rest-frame ultraviolet (observed by the WFC3 near-infrared filters). However, there is no uniform sensitivity over the redshift range probed by the Y band drop-out technique; at the lower redshifts, the $Y - J$ colour might be too blue to enter our selection, and at the higher redshift end of our range the effect of the Lyman α forest means that an increasingly large fraction of the J -band filter is absorbed, so only the most UV-luminous galaxies will appear in our apparent-magnitude-limited sample. We quantify this effect and hence constrain the luminosity function through our observed number counts. The probability of recovering a high-redshift galaxy as a function of redshift and rest-frame UV luminosity can be found with simulations. To perform these simulations, we add into the images a large number of fake galaxies, with properties similar to those of the observed high-redshift population (i.e. compact with half-light radii $r_{\text{hl}} \approx 0.1$ arcsec, large Lyman α forest decrement of $D_A \approx 0.99$ and blue rest-frame UV colours). We then run our selection procedure and infer the probability of recovering such galaxies as a function of redshift and magnitude (see Fig. 5). We adopt the effective volume approach as described in Steidel et al. (1999) and Stanway et al. (2003), such that the probability of recovering a galaxy in our survey depends on the redshift and absolute UV magnitudes, $p(M_{\text{UV}}, z)$, and from this the effective survey volume can be calculated (V_{eff}). We use a Gaussian distribution of spectral slopes, with $\langle \beta \rangle = -2.2$ and $\sigma(\beta) = 0.5$, reflecting the generally blue spectral slopes observed in LBGs at $z \geq 6$ (Stanway, McMahon & Bunker 2005; Bouwens et al. 2010b; Bunker et al. 2010; Wilkins et al. 2011b). In Table 3 we have presented our list of candidate Y -drops, with colours consistent with being high redshift. These are good targets for spectroscopy, but in calculating the luminosity function we wish to restrict the sample to only the most reliable sources (to minimize biases through contamination

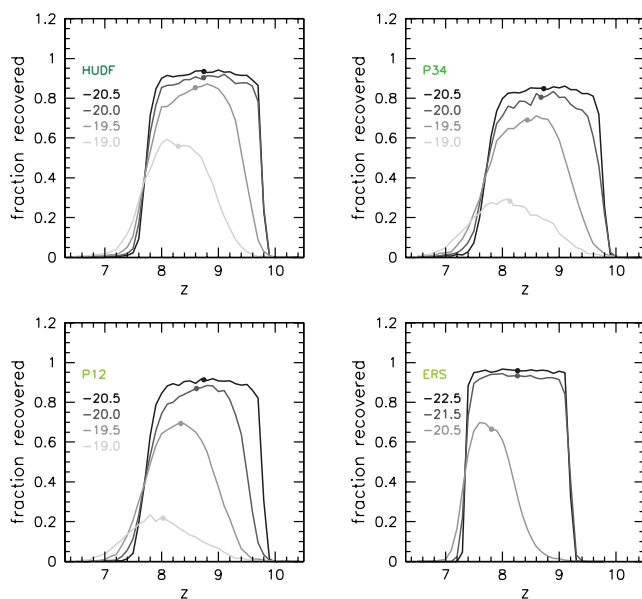


Figure 5. The probability of recovering simulated galaxies as a function of redshift and absolute rest-UV magnitude (M_{1600}). We have run simulations on all four of our fields. The mean redshift is denoted by a dot.

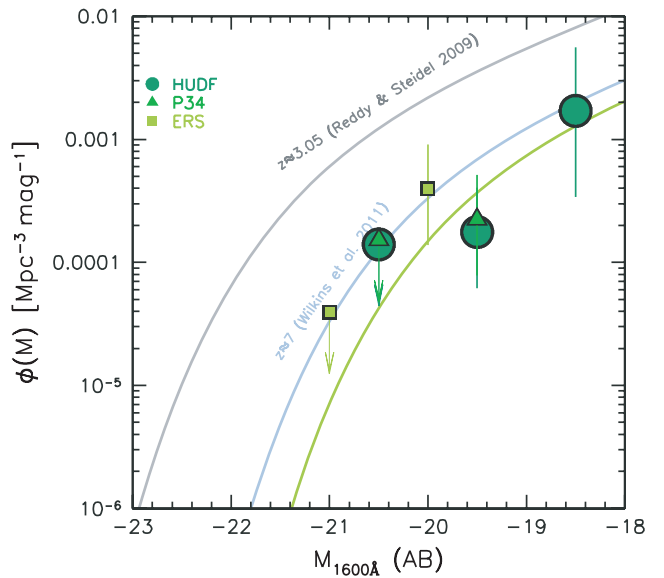


Figure 6. The $z \approx 8-9$ rest-frame UV (1600 Å) luminosity function derived from HUDF, UDF-P34 and ERS WFC3 fields (circles, triangles and squares, respectively) together with contemporary and lower redshift comparisons. Solid lines denote the luminosity function at $\langle z \rangle = 3.05$ (Reddy & Steidel 2009) and $\langle z \rangle \approx 7.0$ (Wilkins et al. 2011a).

by photometric scatter). In determining the luminosity function, we do not consider the P12 Y -drops, where the shallow H band means we do not have secure H -band magnitudes. For the other fields, we include only those galaxies from Table 3 detected at $\geq 7\sigma$ in J band which are not flagged as marginal; the only galaxies at $>7\sigma$ in J band not included in the luminosity function fits are ERS.YD2 and ERS.YD7.

We can then determine the best-fitting luminosity function (Fig. 6); we assume a Schechter (1976) functional form, where the number density of galaxies between L and $L + \delta L$ is

$$\phi(L) dL = \phi^* e^{-x} x^\alpha,$$

where $x = L/L^*$. The Schechter function is parametrized by a faint-end slope (α), a characteristic number density at the knee of the luminosity function (ϕ^*) and the characteristic luminosity, L^* , corresponding to the absolute magnitude in the rest-frame UV (M_{UV}^* , determined around 1600 Å). Unfortunately, we still do not have enough faint galaxies to constrain the faint-end slope of this function, so we adopt three different values for the faint-end slope, $\alpha = -1.5, -1.7, -1.9$, bracketing the value of $\alpha = -1.73$ derived by Bouwens et al. (2006) for the i' -drops at $z = 6$ and for the $z = 3$ U -drops (Reddy & Steidel 2009). We fit for the free parameters ϕ^* and M_{UV}^* , and these are presented in Table 6.

4.2 Evolution of the luminosity function with redshift

We now compare our measured best-fitting luminosity function parameters (Table 6) with previous estimates from the $z \approx 8-9$ galaxies in the HUDF alone. We also plot the $z = 7$ UVLF from the z -drops of Wilkins et al. (2011a), and note that other luminosity functions based on smaller data sets have derived similar parameters (e.g. McLure et al. 2010; Oesch et al. 2010; Ouchi et al. 2010). Based on five Y -drops, Bouwens et al. (2010a) estimated $M_{\text{UV}}^* = -19.45$, assuming no evolution in ϕ^* and α from $z \approx 6$ (fixing $\phi^* = 0.0011 \text{ Mpc}^{-3}$ and $\alpha = -1.74$). This is consistent with our

Table 6. The best-fitting values of M_{1600}^* and ϕ^* for a Schechter function assuming fixed $\alpha \in \{-1.5, -1.7, -1.9\}$ together with the UV luminosity densities (and SFR densities in parentheses) determined by integrating the luminosity function down to various limiting absolute magnitudes.

| α | M_{1600}^* (AB mag) | ϕ^* (Mpc^{-3}) | $\rho_{1600} (10^{25} \text{ erg s}^{-1} \text{ Mpc}^{-3} \text{ Hz}^{-1}) [\rho_* (\text{M}_\odot \text{ yr}^{-1} \text{ Mpc}^{-3})]$ | | |
|----------|-----------------------|--------------------------------|----------------------------------------------------------------------------------------------------------------------------------------|------------------------------------------------|--------------------------------------------------|
| | | | $M_{1600} < -18.5$ (SFR $> 1.5 \text{ M}_\odot \text{ yr}^{-1}$) | $<-13 (>0.01 \text{ M}_\odot \text{ yr}^{-1})$ | $<-8 (>10^{-4} \text{ M}_\odot \text{ yr}^{-1})$ |
| -1.5 | -19.34 | 0.00117 | 1.65 (0.0022) | 4.61 (0.0060) | 4.88 (0.0064) |
| -1.7 | -19.5 | 0.00093 | 1.71 (0.0022) | 6.22 (0.0081) | 7.27 (0.0095) |
| -1.9 | -19.66 | 0.00070 | 1.73 (0.0023) | 9.05 (0.0119) | 13.46 (0.0176) |

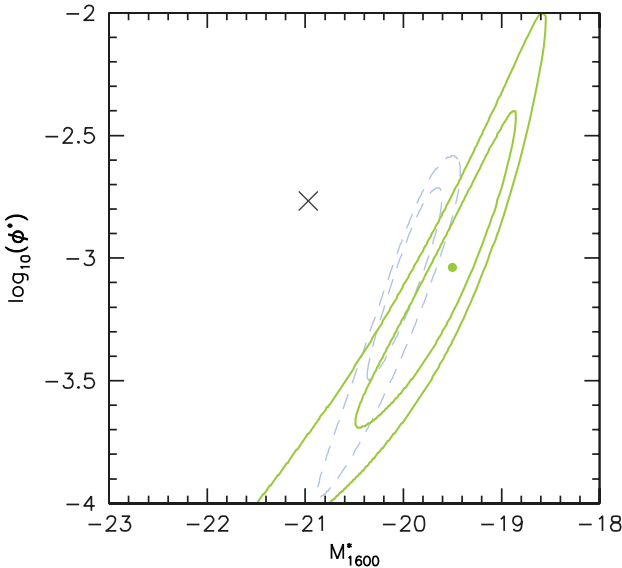


Figure 7. The significance contours for the reduced- χ^2 fits of the Schechter UVLF for the Y -drops (solid contours on right, signifying 1 and 2 sigma significance contours for the inner and outer). A faint-end slope of $\alpha = -1.7$ has been assumed, and the dot is the formal best fit, with $M_{1600}^* = -19.5$ (AB). The dashed contours (to the left of the $z = 8$ contours) denote the $z = 7$ luminosity function derived by Wilkins et al. (2011a) from the z -drops in the same WFC3 fields as analysed here. The cross (on the left) is the $z = 3$ luminosity function for LBGs (Reddy & Steidel 2009). Evolution predominantly in M^* is most consistent with the observational data.

determination of $\phi^* = 0.00093 \text{ Mpc}^{-3}$ and $M_{\text{UV}}^* = -19.5$ (where we have fixed $\alpha = -1.7$ but fit both ϕ^* and M_{UV}^*). We note that our measured characteristic number density is within ≈ 20 per cent of the Bouwens et al. assumption, with M_{UV}^* nearly the same as the Bouwens et al. fit. McLure et al. (2010) suggest that the main luminosity function evolution from $z \approx 6$ is in ϕ^* , with M_{UV}^* broadly unchanged at $M_{\text{UV}} = -20$, and $\phi_{z=6}^* \approx 5 \times \phi_{z=8}^*$. However, this appears to be marginally inconsistent with our number counts of Y -drops at the bright end – this parameter space is unavailable using the HUDF alone, but the larger volume we have in our current study enables us to fit both ϕ^* and M_{UV}^* at $z \approx 8$ – each of the six independent points in the luminosity function (Fig. 6) has ≈ 3 galaxies in it (rather than two bins of 2–3 galaxies previously). The McLure et al. (2010) pure-density-evolution scenario lies on the 1σ contour of our ϕ^* versus L^* reduced- χ^2 plot (Fig. 7). Our results are entirely consistent with an evolution mainly in M_{UV}^* since $z = 7$ (and indeed since $z = 3$), with only a modest change in ϕ^* (consistent with no change in ϕ^*).

The integration of the luminosity function gives us the ultraviolet luminosity density, which is important for our purposes, since it is directly connected with the SFR density. Fig. 8 shows the UV luminosity density as a function of the magnitude down to which

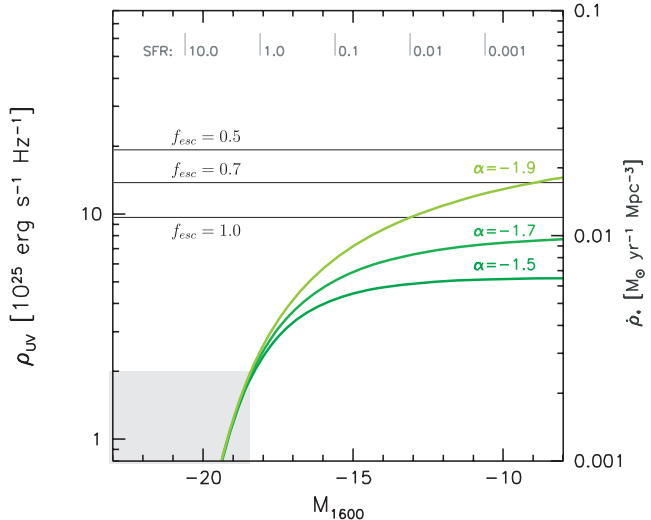


Figure 8. The UV luminosity density (left axis) and SFR density (right axis) as a function of the rest-UV (M_{1600}) absolute magnitude down to which the luminosity function is integrated. We show our best-fitting luminosity functions at $z \approx 8$ –9 assuming $\alpha = -1.5, -1.7, -1.9$. The shaded grey box denotes the observed region with the remainder inferred from extrapolation of the luminosity function. The horizontal lines show the UV luminosity density required to reionize the Universe at this redshift, assuming a clumping factor of $C = 5$, and an escape fraction of $f_{\text{esc}} = 0.5$ (top line), 0.7 (middle) and 1 (bottom).

the luminosity function is integrated for each of the three best fits (one for each value of α adopted).

4.3 The SFR density at $z \approx 8$

We can use the observed H -band magnitudes of objects in the Y -drop sample to estimate their SFR from the rest-frame UV luminosity density around $\lambda_{\text{rest}} = 1600 \text{ \AA}$. In the absence of dust obscuration, the relation between the flux density in the rest-UV around this wavelength and the SFR (in $\text{M}_\odot \text{ yr}^{-1}$) is given by $L_{\text{UV}} = 8 \times 10^{27} \text{ SFR erg s}^{-1} \text{ Hz}^{-1}$ from Madau, Pozzetti & Dickinson (1998) for a Salpeter (1955) stellar initial mass function (IMF) with $0.1 \text{ M}_\odot < M_* < 125 \text{ M}_\odot$. This is comparable to the relation derived from the models of Leitherer & Heckman (1995) and Kennicutt (1998). However, if a Scalo (1986) IMF is used, the inferred SFRs will be a factor of ≈ 2.5 higher for a similar mass range. In the absence of a spectroscopic redshift, we assume that these lie at the predicted average redshift for galaxies obeying our colour cuts (Fig. 5). For the luminosity functions considered, the predicted mean redshift is around $\langle z \rangle = 8.6$ for a spectral slope $\beta \approx -2$ and $M_{\text{UV}} = -20.5$. The H band probes the rest-UV above Lyman α , and is unaffected by the forest absorption. Our 6σ limit for the HUDF is $H_{\text{AB}} = 28.5$, equivalent to an absolute magnitude of $M_{1600 \text{ \AA}} = -18.6$ at $z = 8.6$, corresponding to an inferred star formation of $1.5 \text{ M}_\odot \text{ yr}^{-1}$. This

is equivalent to $0.1 L_{\text{z}=3}^*$ for $M_{\text{UV}}^* = -20.97$ at $z = 3$ (Reddy & Steidel 2009).

With our measured Schechter luminosity function parameters ($\phi^* = 0.00093 \text{ Mpc}^{-3}$, $M^* = -19.5$ assuming $\alpha = -1.7$ at $z = 3$ and 6), the total SFR density is $0.0022 \text{ M}_\odot \text{ yr}^{-1} \text{ Mpc}^{-3}$ integrating down to our luminosity limit of $M_{1600\text{\AA}}^{\text{UV}} \approx -18.5$ mag (AB). This should be regarded as a robust *lower limit* on the SFR density, as dust obscuration may affect the rest-frame UV continuum, and also galaxies fainter than our selection limit will also contribute to the integrated UV light density. If instead we integrate down to $M_{1600\text{\AA}}^{\text{UV}} = -13$ (corresponding to $0.01 \text{ M}_\odot \text{ yr}^{-1}$) and the total SFR density is $0.0081 \text{ M}_\odot \text{ yr}^{-1} \text{ Mpc}^{-3}$. These SFR densities are a factor of ~ 10 lower than at $z \sim 3$ –4, and even a factor of ≈ 3 –5 below that at $z \approx 6$ (Bunker et al. 2004; Bouwens et al. 2006).

4.4 Implications for reionization

The ionizing UV photons produced by the most massive (OB) stars might be critical in reionizing and keeping the Universe ionized at $z \approx 6$ –11. However, work at $z \approx 6$ has shown that under standard assumptions of the IMF, escape fraction and clumping of the gas, the observed population of LBGs produces insufficient flux down to $\text{AB} \approx 28.5$ mag (Bunker et al. 2004), and the ‘photon drought’ is even more severe at $z \approx 7$ (Wilkins et al. 2011a). We now compare our measured UV luminosity density at $z \approx 8$ –9 (quoted above as a corresponding SFR density) with that required to ionize the Universe at this redshift. Madau, Haardt & Rees (1999) give the density of star formation required for reionization (assuming the same Salpeter IMF as used in this paper):

$$\dot{\rho}_{\text{SFR}} \approx \frac{0.012 \text{ M}_\odot \text{ yr}^{-1} \text{ Mpc}^{-3}}{f_{\text{esc}}} \left(\frac{1+z}{1+8.6} \right)^3 \left(\frac{\Omega_b h_{70}^2}{0.0462} \right)^2 \left(\frac{C}{5} \right).$$

We have updated equation (27) of Madau et al. (1999) for a more recent concordance cosmology estimate of the baryon density from Larson et al. (2011), $\Omega_b h_{100}^2 = 0.022622$. The reionization requirement at $z \approx 8.6$ is a factor of 2.5 times higher than that at $z \approx 6$, as the number of photons needed rises as $(1+z)^3$.

In the above equation, C is the clumping factor of neutral hydrogen, $C = \langle \rho_{\text{H}_2}^2 \rangle / \langle \rho_{\text{H}_2} \rangle^{-2}$. Early simulations suggested $C \approx 30$ (Gnedin & Ostriker 1997), but more recent work including the effects of reheating implies a lower concentration factor of $C \approx 5$ (Pawlik, Schaye & van Scherpenzeel 2009). The escape fraction of ionizing photons (f_{esc}) for high-redshift galaxies is highly uncertain (e.g. Steidel, Pettini & Adelberger 2001; Shapley et al. 2006), and it is possible that the escape fraction of ionizing photons may be linked to the escape fraction of Lyman α photons (Stark et al. 2010), which may mean that high escape fractions could be tested through future line emission line searches with spectroscopy and narrow-band imaging. Even if we take the upper limit of $f_{\text{esc}} = 1$ (no absorption by H i) and a very low clumping factor, the required total SFR density for reionization is $0.012 \text{ M}_\odot \text{ yr}^{-1} \text{ Mpc}^{-3}$. This is a factor of ~ 5 higher than our measured star formation density at $z \approx 8$ –9 from Y -drop galaxies brighter than $M_{\text{UV}} = -18.5$ (our approximate limit). As shown in Table 6 and Fig. 8, the required UV luminosity density can only just be achieved (if $f_{\text{esc}} = 1$) by integrating down to $M_{\text{UV}} = -13$ (i.e. extrapolating the Schechter function to ≈ 100 times fainter than our observed limit) and then only for a steeper faint-end slope of $\alpha = -1.9$ rather than $\alpha = -1.7$. Adopting a less unrealistic value of $f_{\text{esc}} = 0.7$ (which is still high compared with observed values at lower redshift) the required total SFR density for reionization would be $0.017 \text{ M}_\odot \text{ yr}^{-1} \text{ Mpc}^{-3}$, then the Y -drop population can only provide sufficient ionizing photons if the faint-

end slope is very steep ($\alpha \leq -1.9$) and the Schechter function is integrated down below $M_{\text{UV}} = -8$ (corresponding to a SFR of only $10^{-4} \text{ M}_\odot \text{ yr}^{-1}$). We note that recent theoretical papers indicate that the reionization process itself may have been ‘photon-starved’ (e.g. Bolton & Haehnelt 2007), consistent with the extrapolation of our observational constraints.

However, the assumption of a solar metallicity Salpeter IMF may be flawed: the colours of $z \sim 6$ i' -band drop-outs are very blue (Stanway et al. 2005), with $\beta < -2$, and the recent WFC3 J - and H -band images show that the $z \approx 7$ z' -drops also have blue colours on average (Bunker et al. 2010; Bouwens et al. 2010b; Wilkins et al. 2011b). Continuous star formation with a Salpeter IMF produces a UV spectral slope of $\beta \approx -2$ if there is no dust reddening. The fact that we observe even more blue slopes than this ($\beta < -2$) could be explained through low metallicity, or a top-heavy IMF, which can produce between 3 and 10 times as many ionizing photons for the same 1600-Å UV luminosity (Schaerer 2003 – see also Stiavelli, Fall & Panagia 2004). Alternatively, we may be seeing galaxies at the onset of star formation, or with a rising SFR (Verma et al. 2007), which would also lead us to underestimate the true SFR from the rest-UV luminosity. We explore the implications of the blue UV spectral slopes in $z \geq 6$ galaxies in a forthcoming paper (Wilkins et al. 2011b).

5 CONCLUSIONS

In this paper we have presented a search for galaxies at $7.5 < z < 10$ using the latest *HST*/WFC3 near-infrared data, based on the Lyman-break technique. Searching for galaxies which have large ($Y - J$) colours (Y -drops) on account of the Lyman α forest absorption, and with ($J - H$) colours inconsistent with being low-redshift contaminants, we identify ≈ 20 candidates at redshift $z \approx 8$ –9 over an area of ≈ 50 arcmin 2 . Our deepest field (the HUDF, covering 4.2 arcmin 2) reaches $J_{\text{AB}} = 28.5$ at 6σ , while the wide-area ERS data (comprising 10 WFC3 pointings covering 37 arcmin 2) reaches $J_{\text{AB}} = 27.2$. The surface densities of candidates as a function of limiting magnitude appear broadly consistent between our four fields, although these all lie within 10 arcmin. Previous searches for Y -drops with WFC3 have focused only on the HUDF, and our larger survey has trebled the number of robust Y -drop candidates, as well as providing a number of brighter Y -drops (with $J_{\text{AB}} \approx 27.0$ rather than $J_{\text{AB}} > 28.0$ as in the HUDF). These brighter sources may be more amenable to spectroscopic follow-up.

For the first time, we have a sufficient number of $z \approx 8$ –9 galaxies to fit ϕ^* and M^* assuming a Schechter luminosity function (previous estimates had to fix one of these parameters). We confirm that there is large evolution from $z = 3$, particularly in the bright end of the luminosity function, in the sense that there are far fewer UV-bright galaxies at $z \approx 8$ –9 than in the more recent past. There is also evidence for evolution from $z = 6$ –7 to 8–9, with this being consistent with most of the change occurring in M^* rather than ϕ^* , with M^* being fainter at higher redshift. We are unable to obtain a good constraint on the faint-end slope, α , which will potentially require deeper data over a wider field (as might be provided by NIRCAM on the *James Webb Space Telescope*). The candidate $z \approx 8$ –9 galaxies we detect have insufficient ionizing flux to reionize the Universe, and it is probable that galaxies below our detection limit provide a significant UV contribution. However, adopting a similar faint-end slope to that determined at $z = 3$ –6 ($\alpha = -1.7$) and a Salpeter IMF, then the ionizing photon budget still falls short if $f_{\text{esc}} < 0.5$, even integrating down to $M_{\text{UV}} = -8$. A steeper faint-end slope and a low-metallicity population (or a top-heavy IMF) might

still provide sufficient photons for star-forming galaxies to reionize the Universe, but confirmation of this might have to await the *James Webb Space Telescope*.

ACKNOWLEDGMENTS

Based on observations made with the NASA/ESA *Hubble Space Telescope*, obtained from the Data Archive at the Space Telescope Science Institute, which is operated by the Association of Universities for Research in Astronomy, Inc., under NASA contract NAS 5-26555. These observations are associated with programme #GO-11563 and #GO/DD-11359. We are grateful to Garth Illingworth and his team, and the WFC3 Science Oversight Committee for making their ERS and *Hubble Ultra Deep Field* observations public. We thank Richard Ellis for useful comments on this paper. MJJ acknowledges the support of a RCUK fellowship. SL and JC are supported by the Marie Curie Initial Training Network ELIXIR of the European Commission under contract PITN-GA-2008-214227. We thank the anonymous referee for helpful comments which have improved this paper.

REFERENCES

- Becker R. H. et al., 2001, AJ, 122, 2850
 Beckwith S. V. W. et al., 2006, AJ, 132, 1729
 Bertin E., Arnouts S., 1996, A&AS, 117, 393
 Bolton J. S., Haehnelt M. G., 2007, MNRAS, 382, 325
 Bouwens R. J., Illingworth G. D., Blakeslee J. P., Franx M., 2006, ApJ, 653, 53
 Bouwens R. J., Illingworth G. D., Franx M., Ford H., 2007, ApJ, 670, 928
 Bouwens R. J., Illingworth G. D., Franx M., Ford H., 2008, ApJ, 686, 230
 Bouwens R. J. et al., 2009, arXiv:0909.1803v1
 Bouwens R. J. et al., 2010a, ApJ, 709, L133
 Bouwens R. J. et al., 2010b, ApJ, 708, L69
 Bunker A., Wilkins S., 2009, arXiv:0912:1351
 Bunker A. J., Stanway E. R., Ellis R. S., McMahon R. G., 2004, MNRAS, 355, 374
 Bunker A. et al., 2010, MNRAS, 409, 855
 Casertano S. et al., 2000, AJ, 120, 2747
 Dunkley J. et al., 2009, ApJS, 180, 306
 Eyles L. P., Bunker A. J., Stanway E. R., Lacy M., Ellis R. S., Doherty M., 2005, MNRAS, 364, 443
 Eyles L. P., Bunker A. J., Ellis R. S., Lacy M., Stanway E. R., Stark D. P., Chiu K., 2007, MNRAS, 374, 910
 Fan X. et al., 2001, AJ, 122, 2833
 Fan X. et al., 2006, AJ, 132, 117
 Ferguson H. C. et al., 2004, ApJ, 600, 107
 Finkelstein S. L., Papovich C., Giavalisco M., Reddy N. A., Ferguson H. C., Koekemoer A. M., Dickinson M., 2010, ApJ, 719, 1250
 Giavalisco M. et al., 2004, ApJ, 600, L103
 Gnedin N. Y., Ostriker J. P., 1997, ApJ, 486, 581
 Gunn J. E., Peterson B. A., 1965, ApJ, 142, 1633
 Hickey S., Bunker A., Jarvis M. J., Chiu K., Bonfield D., 2010, MNRAS, 404, 212
 Kennicutt R. C., 1998, ARA&A, 36, 189
 Knapp G. R. et al., 2004, AJ, 127, 3553
 Koekemoer A. M., Fruchter A. S., Hook R. N., Hack W., 2002, hstc.conf, 337
 Larson D. et al., 2011, ApJS, 192, 16
 Leitherer C., Heckman T. M., 1995, ApJS, 96, 9
 Leitherer C. et al., 1999, ApJS, 123, 3
 McLure R. J., Dunlop J. S., Cirasuolo M., Koekemoer A. M., Sabbi E., Stark D. P., Targett T. A., Ellis R. S., 2010, MNRAS, 403, 960
 Madau P., Pozzetti L., Dickinson M., 1998, ApJ, 498, 106
 Madau P., Haardt F., Rees M., 1999, ApJ, 514, 648
 Oesch P. A. et al., 2007, ApJ, 671, 1212
 Oesch P. A. et al., 2009, ApJ, 690, 1350
 Oesch P. A. et al., 2010, ApJ, 709, L21
 Oke J. B., Gunn J. E., 1983, ApJ, 266, 713
 Ouchi M. et al., 2010, ApJ, 723, 869
 Pawlik A. H., Schaye J., van Scherpenzeel E., 2009, MNRAS, 394, 1812
 Reddy N. A., Steidel C. C., 2009, ApJ, 692, 778
 Salpeter E. E., 1955, ApJ, 121, 161
 Scalo J. M., 1986, Fundamentals Cosmic Phys., 11, 1
 Schaerer D., 2003, A&A, 397, 527
 Schechter P., 1976, ApJ, 203, 297
 Scheuer P. A. G., 1965, Nat, 207, 963
 Schlegel D. J., Finkbeiner D. P., Davis M., 1998, ApJ, 500, 525
 Shapley A. E., Steidel C. C., Pettini M., Adelberger K. L., Erb D. K., 2006, ApJ, 651, 688
 Stanway E. R., Bunker A. J., McMahon R. G., 2003, MNRAS, 342, 439
 Stanway E. R., McMahon R. G., Bunker A. J., 2005, MNRAS, 359, 1184
 Stanway E. R., Bremer M. N., Squitieri V., Douglas L. S., Lehnert M. D., 2008, MNRAS, 386, 370
 Stark D. P., Bunker A. J., Ellis R. S., Eyles L. P., Lacy M., 2007, ApJ, 659, 84
 Stark D. P., Ellis R. S., Bunker A., Bundy K., Targett T., Benson A., Lacy M., 2009, ApJ, 697, 1493
 Stark D. P., Ellis R. S., Chiu K., Ouchi M., Bunker A. J., 2010, MNRAS, 408, 1628
 Steidel C. C., Giavalisco M., Pettini M., Dickinson M., Adelberger K. L., 1996, ApJ, 462, 17
 Steidel C. C., Adelberger K. L., Giavalisco M., Dickinson M., Pettini M., 1999, ApJ, 519, 1
 Steidel C. C., Pettini M., Adelberger K. L., 2001, ApJ, 546, 665
 Stiavelli M., Fall S. M., Panagia N., 2004, ApJ, 610, L1
 Verma A., Lehnert M. D., Förster Schreiber N. M., Bremer M. N., Douglas L., 2007, MNRAS, 377, 1024
 Wilkins S. M., Bunker A. J., Ellis R. S., Stark D., Stanway E. R., Chiu K., Lorenzoni S., Jarvis M. J., 2010, MNRAS, 403, 938
 Wilkins S. M., Bunker A. J., Lorenzoni S., Caruana J., 2011a, MNRAS, 411, 23
 Wilkins S. M. et al., 2011b, MNRAS, submitted
 Yan H., Windhorst R. A., 2004, ApJ, 612, L93
 Yan H., Windhorst R., Hathi N., Cohen S., Ryan R., O'Connell R., McCarthy P., 2010, Res. Astron. Astrophys., 10, 867
 Yoshida M. et al., 2006, ApJ, 653, 988

This paper has been typeset from a \TeX / \LaTeX file prepared by the author.